Research Square

Preprints are preliminary reports that have not undergone peer review.
They should not be considered conclusive, used to inform clinical practice,
or referenced by the media as validated information.

Visualization neuroinflammation in the brain of patients with neuronal intranuclear inclusion disease by TSPO-PET

Ruiqing Ren
Zhongshan Hospital Fudan University
Jing Wang
Zhongshan Hospital Fudan University
Shaoping Zhong
Zhongshan Hospital Fudan University
Yuzhe Li
Shanghai Medical University: Fudan University
Qingyu Lin
Shanghai Clinical Research and Trial Center
Kaiyuan Shen
Zhongshan Hospital Fudan University
Jingzhen Liang
Zhongshan Hospital Fudan University
Yuchen Gong
Shanghai Jiao Tong University school of biomedical engineering
Dengfeng Cheng
Shanghai Clinical Research and Trial Center
Puming Zhang
Shanghai Jiao Tong University School of Biomedical Engineering
Xin Wang
Zhongshan Hospital Fudan University
JING DING
ding.jing@zs-hospital.sh.cn

Zhongshan Hospital Fudan University https://orcid.org/0000-0001-5135-4210

Research Article

Keywords: Neuronal intranuclear inclusion disease, neuroinflammation, 18-kD translocator protein, PET

Posted Date: July 1st, 2026

DOI: https://doi.org/10.21203/rs.3.rs-9592039/v1

License: This work is licensed under a Creative Commons Attribution 4.0 International License. Read Full License

Abstract

Background

Neuronal intranuclear inclusion disease (NIID) is a progressive neurodegenerative disorder, with neuroinflammation believed to be a key driver. PET radioligands targeting the 18-kDa translocator protein (TSPO) serve as in vivo markers of neuroinflammation. This study aimed to evaluate TSPO-PET in assessing neuroinflammation severity in NIID and to investigate its relationship with clinical features, using [^{11}C]-ER176 and [^{18}F]-FDG PET/MR in ten NIID patients and five epilepsy controls.

Results

TSPO-PET standard uptake value ratios (SUVR) were significantly elevated in NIID patients compared to controls, regardless of brain template used ($p < 0.01$). TSPO-PET SUVR of superficial white matter was negatively correlated with fractional anisotropy ($R = -0.817$, $p < 0.05$). No significant differences in SUVR were found among NIID subgroups based on modified Rankin scale score ≥ 4, NOTCH2NLC GGC repeats ≥ 110, onset age, or encephalitis syndrome.

Conclusions

This study demonstrates that increased neuroinflammation is closely linked to white matter fiber damage. These findings highlight the role of inflammation in NIID pathophysiology and suggest TSPO-PET as a valuable tool for monitoring disease progression.

Introduction

Neuronal intranuclear inclusion disease (NIID) is a progressive neurodegenerative disease with relatively high prevalence in East Asians and clinical, pathological, and radiological similarities to fragile X-associated tremor/ataxia syndrome (FXTAS)(1, 2). In 2019, research groups from China and Japan identified expanded GGC repeats in the 5 'untranslated region (UTR) of human specific NOTCH2NLC gene as the cause of this disease(3–7). The clinical manifestations of NIID are complicated, usually including cognitive decline(3), tremor, paroxysmal symptoms, and autonomic nervous system dysfunction(8). The pathological features of NIID are widespread eosinophilic intranuclear inclusions seen in multiple systems(8). Symmetrical hyperintensity detected by diffusion-weighted imaging (DWI) along the corticomedullary junction (CMJ) in MRI is considered as a diagnostic indicator of this disease(8, 9).

Neuroinflammation is an important contributor on the progression of numerous neurodegenerative diseases(10). Previous autopsy studies have reported reactive astrocytes and microglia in the white matter of NIID patients, which are pathogenic markers of neuroinflammation(11, 12). Our recent research has confirmed the role of microglia in exacerbating NIID pathology in a mouse model(13). However, these findings have not yet been adequately validated in living patients. PET targeting the 18-kDa translocator protein (TSPO), also known as the peripheral benzodiazepine receptor (PBR), is the most widely-used technology for visualizing neuroinflammation in-vivo(14). TSPO intensity correlates with microglial cell density and activation levels in the brain(15), and has been shown to be increased in many neurodegenerative diseases, such as Alzheimer's disease (AD)(16), Parkinson's disease (PD)(17, 18), Huntington's disease (HD)(19). In addition, TSPO-PET is used to monitor the recurrence and progression of inflammatory brain diseases such as multiple sclerosis (MS)(20).

In this study, we performed TSPO-PET combined with MRI scans on 10 patients with adult-onset NIID. We observed an elevated standardized uptake value ratio (SUVR) of TSPO-PET throughout their brain. Diffusion tensor imaging (DTI)-related indicators were identified, revealing a positive correlation between TSPO expression levels and the extent of white matter lesions across the brain. Moreover, we analyzed the distribution characteristics of TSPO-PET SUVR among different

NIID subgroups and elucidated the relationships between cerebral neuroinflammation and clinical features in NIID patients. Our study demonstrated elevated neuroinflammation levels in NIID brains and suggests TSPO-PET is a useful imaging method to monitor disease progression of NIID.

Materials and methods

Participants

Patients diagnosed as NIID from May 2019 to Sep 2022 at the department of neurology, Zhongshan hospital, Fudan University were included in this study. Following criteria were used for the diagnose of NOTCH2NLC-related NIID according to previous studies(4, 6): (1) patients with previously reported clinical manifestations of NIID; (2) with extensive and bilateral white matter lesions on MRI; (3) with NOTCH2NLC GGC repeat size over 60 confirmed by genetic tests; (4) with p62- and ubiquitous-positive intranuclear inclusions detected in the tissues (if pathological examinations were available). This study was approved by the Ethics Committee of Zhongshan Hospital, Fudan University (Approval ID: B2021-286). Informed consent was signed by all participants according to the Declaration of Helsinki. Detailed clinical data and family histories of the participants were collected. Encephalitis-like episode was defined as a series of acute-onset neurological manifestations exhibiting typical features of encephalitis, including altered mental status, seizures, and focal neurological deficits. Neurological physical examination was performed by experienced neurologists. MRI scans and other auxiliary examinations were conducted according to clinical routine in Zhongshan hospital.

Genetic test

Genomic DNA of NIID patients was extracted from fresh blood using a commercial kit (DP349, TIANGEN). Repeat-primed PCR (RP-PCR) and amplicon-length PCR (AL-PCR) performed as previously described. Electrophoresis was performed on a 3700xl Genetic analyzer and the data were analyzed by GeneMarker software (version 2.6.3). A saw-tooth tail pattern in the electropherogram of RP-PCR was considered as the disease-associated repeat expansion.

PET/MR imaging

Production and quality control of [¹¹C]-ER176

HM-20E positron cyclotron was used to produce 11C with nitrogen-oxygen mixture of 1% O2, beam current of 40μA and bombardment for 20min. Labeling of ER176: 0.5mL 0.2M LiAlH4 (THF) was added to flask 1 with 11CO2 made by the accelerator to produce 11CH3OIi. Then 0.4mL 55–57% HI (aq) was added to produce 13CH3I. Afterwards it was heated and transferred to flask 2 to react with pre-ER176. [¹¹C]-ER176 injection was obtained by preparative HPLC after separation through aseptic membrane. Radioactive HPLC was adopted to identify the products and radioactive impurities of the markers. Chemical purity was set to be ≥ 95%.

Subject imaging

[¹¹C]-ER176 PET/MRI imaging: Patients fasted for at least 6 hours before the examination. [¹¹C]-ER176 740 MBq (20 mCi) was slowly injected intravenously into the patients. Dynamic acquisition of the images was conducted at once for 1 hour. Acquisition was 3D mode. Scan lasted for 15 min, in sync with MRI scan. Scanning parameters: field of view (FOW) 25 cm×25 cm, matrix 344×344, iteration number 8, subset number 21, half-height and width 4 mm, reconstruction type Gaussian, attenuation correction by MRAC, attenuation correction by MR u-map. List mode was selected for image reconstruction. MRI scanning parameters: Sag 3D T1W1 (TR 1900 ms, TE 2.53ms, FOV 25 cm×25 cm, matrix 256×256, layer thickness 1 mm, layer spacing 0 mm), Ax T2WI (TR 4000 ms, TE 102 ms, NEX 2, FOV 220 mm×220 mm, matrix

320×320, layer thickness 5 mm, layer spacing 1.5 mm), 3D fluid attenuated inversion recovery (FLAIR) (TR 5 000 ms, TE 395 ms, matrix 256×256, layer thickness 1 mm, layer spacing 0 mm), SPC DIR and DTI. Patients fasted for at least 6 hours before the examination. The injection method, dynamic acquisition duration, imaging instruments and parameters were the same as [^{11}C]-ER176 PET/MRI imaging.

Image Preprocessing

All PET (TSPO-PET and FDG-PET) and MRI (T1-weighted, T2-FLAIR and DWI) images were registered to Montreal Neurological Institute (MNI) space and resliced as a resolution of 1 mm. PET images were smoothed by a 3 mm full-width at half-maximum (FWHM) Gaussian kernel. Standard uptake value ratio (SUVR) of PET image was calculated as the ratio of brain uptake in target regions compared with that in the cerebellum, where served as the reference region to minimize errors added by measurement of plasma concentrations(21, 22).

For the following analyses, we defined two whole-cerebrum masks, an Anatomical Automatic Labeling (AAL)-based mask and an individual mask. The AAL-based mask was defined by a standard template in the MNI space, AAL atlas, covering all the 90 AAL regions in cerebrum(23). The individual masks were personalized on the shape of grey matter and white matter in each sample. Individual grey matter and white matter masks were generated by integrating automatic segmentation results of T1-weighted, T2-FLAIR and DWI images, then merged into the individual whole-cerebrum masks. Cerebellum and brainstem were removed from these masks.

DTI data was preprocessed through MRtrix3 toolbox, briefly including denoising, removal of Gibbs artifacts, eddy-current correction and registration to the MNI space. Two maps of diffusion tensor-derived parameters, fractional anisotropy (FA) and mean diffusivity (MD), were generated after preprocessing(24). FA and MD maps were resliced with a voxel size of 1 × 1 × 1 mm3 and smoothed by the 3 mm FWHM Gaussian kernel.

Statistical Parametric Mapping (SPM12, http://www.fil.ion.ucl.ac.uk/spm/software/spm12/) software was used for registration, smoothing and segmentation on Matlab R2021b (MathWorks Inc., Natick, MA, USA). MRtrix3 was performed in Ubuntu 18.04 environment.

Variables Collection and Assessment of PET Examination

To assess the performance of TSPO-PET and FDG-PET in NIID investigation compared to epilepsy controls, we calculated z-scores of NIIDs, by subtracting the mean value of controls then being divided by the standard deviation of controls, and the average of SUVRs from preprocessed PET images within the AAL-based whole-cerebrum masks, which represented global SUVR at the whole cerebrum level. No patient data was excluded in this step. Mean SUVRs of the whole grey and white matters were also extracted after excluding Patient 3 for its poor quality of structural MRI images to segment distinct grey matter and white matter. We compared global SUVR difference between NIIDs and epilepsy controls, within the grey matter, white matter and individual whole-cerebrum mask, respectively.

Besides analyses between NIIDs and epilepsy controls, we subdivided NIID patients into two subgroups by three clinical characteristics (encephalitis syndrome, MRS score ≥ 4, NOTCH2NLC GGC repeats ≥ 110) and calculated the TSPO-PET SUVR and FDG-PET SUVR difference between NIID subgroups. Furthermore, the correlation between global TSPO-PET SUVR and two DTI diffusivity measures of NIIDs, FA and MD, was examined within the overlapping of the AAL-based whole cerebrum mask and individual white matter masks.

Statistical Analysis

The statistically significant difference between NIIDs and epilepsy controls, and between NIID subgroups, was calculated by a nonparametric Mann-Whitney U test because of the non-normal distribution and small sample of data. We calculated

Spearman's correlation coefficient between TSPO-PET SUVR and two diffusivity measures, FA and MD. All statistical significance was defined as $p < 0.05$.

Results

Clinical features of the NIID Patients

We enrolled 10 Chinese adults diagnosed with NIID, including 3 males and 7 females, aged 52 to 71 years (Table 1). The mean age of onset was 61.4 ± 6.2 years. Disease duration ranged from 1 to 13 years. Most patients presented with headache (33.33%) and cognitive decline (33.33%) as the Initial clinical manifestations. Tremor (20%) and autonomic dysfunction (10%) were frequently seen. Encephalitis-like episode, a characteristic presentation of NIID with reversible attacks of fever, nausea, vomiting, headache, and disturbance of consciousness, was observed in three patients (Patient 1, 2, and 5). These diverse symptoms highlight the complexity NIID manifestations and its broad impact on both the central nervous system and other organs. Disability level was assessed using the Modified Rankin Scale (MRS), averaged 3.5 ± 1.5 among these patients. Cognitive impairment was observed in 6 out of 10 patients, with memory and executive function notably affected. Mini-Mental State Examination (MMSE) assessments was 18.3 ± 8.2, though data for Patient 6 were unavailable due to symptom deterioration. All patients had more than 60 GGC repeats in the NOTCH2NLC gene, with a median of 110.5 repeats.

Table 1
Demographic and clinical Features of NIID patients

Patient No.	Sex	Onset age	First manifestation	Disease duration	MRS score	MMSE score	Encephalitis-like episode	NOTCH2NLC GGC repeats
P1 (72 year)	Female	71	Headache	1yr	4	16	+	140
P2 (62 year)	Female	62	Episodic headache with vomiting	4yr	3	16	+	115
P3 (66 year)	Female	55	Episodes of involuntary movements of the limbs	12yr	5	7	-	109
P4 (66 year)	Male	65	Cognitive decline	1yr	2	28	-	305
P5 (66 year)	Female	63	Difficulty urinating, unresponsiveness	3yr	4	9	+	110
P6 (59 year)	Male	52	Headache	7yr	4	Unable to assess	-	102
P7 (69 year)	Female	65	Episodes of impaired consciousness	4yr	1	28	-	89
P8 (68 year)	Female	66	Cognitive decline	2yr	2	27	-	211
P9 (73 year)	Male	62	Cognitive decline	11yr	6	12	-	86
P10 (66 year)	Female	53	Tremor	13yr	4	22	-	111

Brain MRI features in NIID patients

Most patients, except P7 and P9, exhibited subcortical lace sign, a hallmark of NIID characterized by symmetrical hyperintensity in diffusion-weighted imaging (DWI) along the corticomedullary junction (CMJ), shown in Fig. 1. Additionally, symmetric and diffuse bilateral white matter hyperintensity was observed on T2 FLAIR, extending from the cerebral deep white matter to brainstem and cerebellum. Cerebral atrophy and bilateral ventricular enlargement were also noted in three cases.

TSPO signal intensity increased in NIID patients

Z-scores for FDG-PET (Fig. 2A) and TSPO-PET (Fig. 2B) SUVRs were calculated for NIID patients relative to an epilepsy control group, serving as a reference for global SUVR across the cerebrum. SUVR analyses were performed using both the AAL standard brain template and an individual gray matter-white matter template. FDG-PET SUVRs were significantly lower in NIID patients compared to controls using the AAL template *($p < 0.01$)* (Fig. 2C), while TSPO-PET SUVRs were significantly higher in NIID patients *($p < 0.01$)* (Fig. 2D). No significant difference was found in FDG-PET SUVR between the groups using

the individual gray matter-white matter template (Fig. 2E). However, values of TSPO-PET SUVR for the whole brain in NIID patients were also significantly elevated compared to the control group *(p < 0.01)* (Fig. 2F). FDG-PET SUVRs in gray matter were significantly lower in NIID patients *(p < 0.01)*, with no differences in white matter (Fig. 2G). TSPO-PET SUVRs in both gray and white matter were elevated in NIID patients *(p < 0.01)* (Fig. 2H). These findings suggest elevated inflammation in NIID.

Correlation between TSPO signal intensity and the severity of white matter lesions

To explore the reasons for the more pronounced imaging results of TSPO compared to FDG, we choose the overlap between the brain areas defined using the AAL standard brain template and those defined using the individual template to derive region of interest, which represents superficial white matter (Fig. 3A). Diffusion tensor imaging (DTI) was used to assess the directional consistency of water molecule diffusion (fractional anisotropy, FA) and the degree of diffusion (mean diffusivity, MD). FA and MD were employed to evaluate global and specific white matter integrity. The NIID group showed significantly lower FA *(p < 0.001)* and higher MD *(p < 0.05)* compared to controls, indicating more severe white matter lesions in NIID patients (Fig. 3B). We further examined the association of FDG and TSPO intensity and white matter lesions revealed by DTI. A correlation analysis of FDG-PET SUVR with FA and MD in 9 patients showed a significant negative correlation between global FDG-PET SUVR and FA *(R=-0.833, p < 0.05)* (Fig. 3C), while no significant correlation was found with MD *(R = 0.35, p = 0.358)* (Fig. 3D). There was also a significant negative correlation between global TSPO-PET SUVR and FA *(R=-0.817, p < 0.05)* (Fig. 3E), while no significant correlation was found with MD *(R = 0.25, p = 0.521)* (Fig. 3F). These results suggest that increased inflammation in NIID patients is closely associated with white matter fiber damage, highlighting inflammation as a key contributor to white matter impairment.

TSPO-PET revealing disease severity

We conducted Spearman's rank correlation analyses to examine relationships between TSPO-PET SUVR values and clinical indicators, including MRS scores, NOTCH2NLC GGC repeat number, and age of onset. We did not detect significant correlations between TSPO intensity and these indicators using neither the AAL standard brain template nor the individual brain template (Fig. 4A-C). However, we observed a trend of increasing TSPO SUVR with higher MRS scores and earlier onset age, though these were also not statistically significant. Furthermore, no significant differences were found between groups with or without encephalitis-like episodes, regardless of the brain template used (Fig. 4D).

Discussion

In this study, we focus on conducting whole-brain SUVR analyses using TSPO-PET and FDG-PET, and examining their associations with white matter damage and clinical characteristics of the NIID patients. Our findings offer novel insights into the pathophysiology of NIID, with potential implications for diagnosis and therapeutic interventions.

The clinical profile of the 10 patients enrolled in this study underscores the multifaceted nature of NIID. The mean age of onset and disease duration are consistent with previous reports of late-onset NIID, which predominantly affects elderly populations(25, 26). The wide spectrum of initial symptoms, including headache, cognitive decline, tremor, and autonomic dysfunction, reflects the broad impact of NIID on the central nervous system (CNS) and peripheral systems. The occurrence of encephalitis-like episodes in 30% of the patients is particularly noteworthy, as these reversible episodes are a hallmark of NIID, often presenting diagnostic challenges. MRI findings in this cohort corroborate the established hallmarks of NIID while shedding light on additional pathological changes. The subcortical lace sign, a diagnostic feature of NIID, was observed on most patients, which is believed caused by spongiform pathological changes in the white matter near the subcortical U fiber(12). T2 FLAIR imaging further revealed extensive bilateral white matter hyperintensity,

extending from the cerebral deep white matter to the brainstem and cerebellum. These findings underscore the pervasive involvement of white matter, consistent with the clinical presentation of cognitive and motor dysfunctions.

TSPO plays a crucial rule in various physiological processes and neurodegenerative diseases, with its expression elevated in activated microglia(15), making it a key biomarker for both acute and chronic neuroinflammation. Numerous PET molecular probes targeting TSPO have been developed, with [¹¹C]-PK11195 being the most effective first-generation TSPO tracer(27). However, it has limitations, including low blood-brain barrier permeability, high levels of nonspecific binding resulting in a low signal-to-noise tatio (SNR), a short half-life, and a poor metabolic profile. Consequently, second-generation TSPO radiotracers, such as [¹¹C]-DAA1106 and [¹¹C]-PBR28, have been developed to address these issues(28, 29). Despite their advancements, genetic polymorphism (rs6971) affects their binding potency, leading to significant individual variability(30, 31). Third-generation TSPO radiotracers have emerged to overcome genetic polymorphism and improved quantitative analysis, including [18F]-GE-18, [¹¹C]-ER176, [¹¹C]-CB184, [18F]-LW223 and [¹¹C]-N '-MPB(32). Among them, [18F]-GE-180(33, 34) and [¹¹C]-ER176(35) have been widely used in preclinical and clinical trials to study neuroinflammation. However, research showed that [^{18}F]-GE-180 had very low brain uptake in human subjects, hindering its translation to human PET imaging(36). Conversely, [¹¹C]-ER176, featuring a quinconazole formamide structure, exhibits high binding affinity for all TSPO rs6971 genotypes(37, 38). To minimize potential limitations, we utilized [¹¹C]-ER176 to quantify PBR in NIID brain and to provide a more precise measurement of neuroinflammation progression.

Our TSPO-PET analyses revealed significantly elevated TSPO signal intensity in NIID patients compared to controls, pointing to heightened neuroinflammation. The increase in TSPO standardized uptake value ratios (SUVRs) across both gray and white matter regions provides compelling evidence of widespread inflammatory activation in NIID. Abnormalities of microglia and astrocytes have been documented in FXTAS and NIID(12, 39, 40). Additionally, previous brain autopsy studies have reported the presence of many GFAP positive reactive astrocytes and CD68 positive microglia and macrophages within the white matter(11). This finding is consistent with previous studies suggesting that microglial activation and astrogliosis are central to the disease's pathophysiology. Interestingly, while FDG-PET SUVRs were reduced in gray matter regions, indicating decreased metabolic activity, no significant differences were observed in white matter. This suggests that while neuronal metabolic dysfunction is pronounced in cortical areas, the inflammatory burden in white matter, as captured by TSPO-PET, is a more prominent feature of NIID. The elevated TSPO-PET SUVRs, even in regions with intact glucose metabolism, underscore the dissociation between inflammation and metabolic dysfunction in NIID.

Diffusion tensor imaging (DTI) provided additional insights into the relationship between inflammation and white matter integrity(41). The significant reductions in fractional anisotropy (FA) and increases in mean diffusivity (MD) in NIID patients indicate compromised white matter fiber integrity. Correlation analyses revealed a significant negative association between global TSPO-PET SUVRs and FA, suggesting that elevated inflammation is closely linked to white matter damage. This finding supports the hypothesis that neuroinflammation is a driving force behind white matter degeneration in NIID(13). The lack of significant correlation between FDG-PET SUVRs and MD further highlights the differential roles of metabolic dysfunction and inflammation in the disease. While metabolic changes may reflect neuronal loss or dysfunction, inflammation appears to be a primary contributor to structural white matter damage, as evidenced by TSPO-PET findings.

Despite the robust imaging findings, correlations between TSPO-PET SUVRs and clinical indicators such as MRS scores, NOTCH2NLC GGC repeat number, and age of onset were not statistically significant. This lack of correlation may reflect the complex interplay of genetic, inflammatory, and degenerative processes in NIID(5), as well as the relatively small sample size in our study. However, the observed trends of higher TSPO SUVRs with increased disability (higher MRS scores) and earlier onset age warrant further investigation in larger cohorts. The absence of significant differences in TSPO-PET SUVRs between patients with and without encephalitis-like episodes suggests that inflammation is a pervasive feature of NIID, irrespective of specific clinical manifestations. This finding highlights the potential of TSPO-PET as a biomarker for disease activity rather than symptom-specific pathology.

Our study has several limitations. First, on account of ethical restrictions, the control group comprised patients with epilepsy rather than healthy individuals. While epilepsy itself is associated with inflammation, the inflammatory activities observed in NIID patients were more pronounced. Second, we did not include post-treatment follow-up data in our analysis, so the results primarily reflect the patients' conditions at the time of admission. Future studies should aim to validate these findings in larger cohorts and explore the longitudinal changes in TSPO-PET signals in relation to clinical progression. Additionally, integrating TSPO-PET with advanced imaging modalities such as functional MRI (fMRI) could provide a more comprehensive understanding of the neuroinflammatory and neurodegenerative processes in NIID.

Conclusion

In conclusion, this study highlights the central role of neuroinflammation in NIID, as evidenced by elevated TSPO-PET signals and their association with white matter damage. The combination of clinical, genetic, and imaging findings underscores the complexity of NIID and the need for multimodal approaches to diagnosis and management. Our results pave the way for further exploration of anti-inflammatory therapies and the development of biomarkers for disease monitoring.

Declarations

Competing interests

The authors declare no competing interests.

Ethics approval

This study was performed in line with the principles of the Declaration of Helsinki. Approval was granted by the Ethics Committee of Zhongshan hospital (Approval Number: B2021-496R).

Consent to participate

Informed consent was obtained from all subjects involved in the study.

Consent for publication

The authors affirm that all human participants involved in this study have signed the consent form and agreed to the publication of their medical imaging.

Funding:

This research was supported by National Key R&D Program of China(Code:2022YFC2503802).

Author Contributions

RR: Methodology, data curation, investigation, writing--original draft, visualization.

JW: Data curation, investigation.

SZ: Data curation, writing--original draft.

YL: Data curation

QL: Preparation and production of [^{11}C]-ER176

KS: Data curation, writing--original draft.

JL: Data curation, investigation.

YG: Methodology, software, validation.

DC: Conceptualization, investigation, project administration.

PZ: Conceptualization, project administration.

XW: Supervision.

JD: Conceptualization, writing--review and editing, project administration.

All authors read and approved the final manuscript.

Acknowledgements:

We are grateful to our patients for their cooperation. We would like to thank the State Key Laboratory of Medical Neurobiology of the Institutes of Brain Science and the Collaborative Innovation Center for Brain Science, and CAS Center for Excellence in Brain Science and Intelligence Technology for supporting the research.

Data availability

Data are available on request from the Department of Neurology, Zhongshan Hospital, Fudan University, Shanghai 200032, China.

References

1. Zhong S, Lian Y, Luo W, Luo R, Wu X, Ji J, et al. Upstream open reading frame with NOTCH2NLC GGC expansion generates polyglycine aggregates and disrupts nucleocytoplasmic transport: implications for polyglycine diseases. Acta Neuropathol. 2021;142(6):1003–23.
2. Gelpi E, Botta-Orfila T, Bodi L, Marti S, Kovacs G, Grau-Rivera O, et al. Neuronal intranuclear (hyaline) inclusion disease and fragile X-associated tremor/ataxia syndrome: a morphological and molecular dilemma. Brain. 2017;140(8):e51.
3. Bao L, Zuo D, Li Q, Chen H, Cui G. Current advances in neuronal intranuclear inclusion disease. Neurol Sci. 2023;44(6):1881–9.
4. Tian Y, Wang JL, Huang W, Zeng S, Jiao B, Liu Z, et al. Expansion of Human-Specific GGC Repeat in Neuronal Intranuclear Inclusion Disease-Related Disorders. Am J Hum Genet. 2019;105(1):166–76.
5. Cao Y, Wu J, Yue Y, Zhang C, Liu S, Zhong P, et al. Expanding the clinical spectrum of adult-onset neuronal intranuclear inclusion disease. Acta Neurol Belg. 2022;122(3):647–58.
6. Sone J, Mitsuhashi S, Fujita A, Mizuguchi T, Hamanaka K, Mori K, et al. Long-read sequencing identifies GGC repeat expansions in NOTCH2NLC associated with neuronal intranuclear inclusion disease. Nat Genet. 2019;51(8):1215–21.
7. Ishiura H, Shibata S, Yoshimura J, Suzuki Y, Qu W, Doi K, et al. Noncoding CGG repeat expansions in neuronal intranuclear inclusion disease, oculopharyngodistal myopathy and an overlapping disease. Nat Genet.

2019;51(8):1222–32.

8. Sone J, Mori K, Inagaki T, Katsumata R, Takagi S, Yokoi S, et al. Clinicopathological features of adult-onset neuronal intranuclear inclusion disease. Brain. 2016;139(Pt 12):3170–86.
9. Silva MS, Fernandes ARC, Cardoso FN, Longo CH, Aihara AY. Radiography, CT, and MRI of Hip and Lower Limb Disorders in Children and Adolescents. Radiographics. 2019;39(4):1232.
10. Zhang W, Xiao D, Mao Q, Xia H. Role of neuroinflammation in neurodegeneration development. Signal Transduct Target Ther. 2023;8(1):267.
11. Liu Y, Mimuro M, Yoshida M, Hashizume Y, Niwa H, Miyao S, et al. Inclusion-positive cell types in adult-onset intranuclear inclusion body disease: implications for clinical diagnosis. Acta Neuropathol. 2008;116(6):615–23.
12. Yokoi S, Yasui K, Hasegawa Y, Niwa K, Noguchi Y, Tsuzuki T, et al. Pathological background of subcortical hyperintensities on diffusion-weighted images in a case of neuronal intranuclear inclusion disease. Clin Neuropathol. 2016;35(6):375–80.
13. Zhong S, Lian Y, Zhou B, Ren R, Duan L, Pan Y, et al. Microglia contribute to polyG-dependent neurodegeneration in neuronal intranuclear inclusion disease. Acta Neuropathol. 2024;148(1):21.
14. Werry EL, Bright FM, Piguet O, Ittner LM, Halliday GM, Hodges JR et al. Recent Developments in TSPO PET Imaging as A Biomarker of Neuroinflammation in Neurodegenerative Disorders. Int J Mol Sci. 2019;20(13).
15. Zhang L, Hu K, Shao T, Hou L, Zhang S, Ye W, et al. Recent developments on PET radiotracers for TSPO and their applications in neuroimaging. Acta Pharm Sin B. 2021;11(2):373–93.
16. Gouilly D, Saint-Aubert L, Ribeiro MJ, Salabert AS, Tauber C, Péran P, et al. Neuroinflammation PET imaging of the translocator protein (TSPO) in Alzheimer's disease: An update. Eur J Neurosci. 2022;55(5):1322–43.
17. Edison P, Ahmed I, Fan Z, Hinz R, Gelosa G, Ray Chaudhuri K, et al. Microglia, amyloid, and glucose metabolism in Parkinson's disease with and without dementia. Neuropsychopharmacology. 2013;38(6):938–49.
18. Lavisse S, Goutal S, Wimberley C, Tonietto M, Bottlaender M, Gervais P, et al. Increased microglial activation in patients with Parkinson disease using [(18)F]-DPA714 TSPO PET imaging. Parkinsonism Relat Disord. 2021;82:29–36.
19. Roussakis AA, Piccini P. PET Imaging in Huntington's Disease. J Huntingtons Dis. 2015;4(4):287–96.
20. Airas L, Rissanen E, Rinne JO. Imaging neuroinflammation in multiple sclerosis using TSPO-PET. Clin Transl Imaging. 2015;3(6):461–73.
21. Dukart J, Mueller K, Horstmann A, Vogt B, Frisch S, Barthel H, et al. Differential effects of global and cerebellar normalization on detection and differentiation of dementia in FDG-PET studies. NeuroImage. 2010;49(2):1490–5.
22. Lyoo CH, Ikawa M, Liow JS, Zoghbi SS, Morse CL, Pike VW, et al. Cerebellum Can Serve As a Pseudo-Reference Region in Alzheimer Disease to Detect Neuroinflammation Measured with PET Radioligand Binding to Translocator Protein. J Nucl Med. 2015;56(5):701–6.
23. Tzourio-Mazoyer N, Landeau B, Papathanassiou D, Crivello F, Etard O, Delcroix N, et al. Automated anatomical labeling of activations in SPM using a macroscopic anatomical parcellation of the MNI MRI single-subject brain. NeuroImage. 2002;15(1):273–89.
24. Tournier JD, Smith R, Raffelt D, Tabbara R, Dhollander T, Pietsch M, et al. MRtrix3: A fast, flexible and open software framework for medical image processing and visualisation. NeuroImage. 2019;202:116137.
25. Tian Y, Zhou L, Gao J, Jiao B, Zhang S, Xiao Q, et al. Clinical features of NOTCH2NLC-related neuronal intranuclear inclusion disease. J Neurol Neurosurg Psychiatry. 2022;93(12):1289–98.
26. Tai H, Wang A, Zhang Y, Liu S, Pan Y, Li K, et al. Clinical Features and Classification of Neuronal Intranuclear Inclusion Disease. Neurol Genet. 2023;9(2):e200057.
27. Benavides J, Quarteronet D, Imbault F, Malgouris C, Uzan A, Renault C, et al. Labelling of peripheral-type benzodiazepine binding sites in the rat brain by using [3H]PK 11195, an isoquinoline carboxamide derivative: kinetic studies and autoradiographic localization. J Neurochem. 1983;41(6):1744–50.

28. Adhikari A, Singh P, Mahar KS, Adhikari M, Adhikari B, Zhang MR, et al. Mapping of Translocator Protein (18 kDa) in Peripheral Sterile Inflammatory Disease and Cancer through PET Imaging. Mol Pharm. 2021;18(4):1507–29.
29. Adhikari A, Zhang MR, Tiwari AK. Acetamidobenzoxazolone scaffold as a promising translocator protein (18 kDa, TSPO) marker for neuroinflammation imaging: Advancement in last decennial period. Drug Dev Res. 2022;83(7):1519–33.
30. Kreisl WC, Jenko KJ, Hines CS, Lyoo CH, Corona W, Morse CL, et al. A genetic polymorphism for translocator protein 18 kDa affects both in vitro and in vivo radioligand binding in human brain to this putative biomarker of neuroinflammation. J Cereb Blood Flow Metab. 2013;33(1):53–8.
31. Zanotti-Fregonara P, Zhang Y, Jenko KJ, Gladding RL, Zoghbi SS, Fujita M, et al. Synthesis and evaluation of translocator 18 kDa protein (TSPO) positron emission tomography (PET) radioligands with low binding sensitivity to human single nucleotide polymorphism rs6971. ACS Chem Neurosci. 2014;5(10):963–71.
32. Singh P, Singh D, Srivastava P, Mishra G, Tiwari AK. Evaluation of advanced, pathophysiologic new targets for imaging of CNS. Drug Dev Res. 2023;84(3):484–513.
33. López-Picón FR, Snellman A, Eskola O, Helin S, Solin O, Haaparanta-Solin M, et al. Neuroinflammation Appears Early on PET Imaging and Then Plateaus in a Mouse Model of Alzheimer Disease. J Nucl Med. 2018;59(3):509–15.
34. Vomacka L, Albert NL, Lindner S, Unterrainer M, Mahler C, Brendel M, et al. TSPO imaging using the novel PET ligand [(18)F]GE-180: quantification approaches in patients with multiple sclerosis. EJNMMI Res. 2017;7(1):89.
35. Appleton J, Finn Q, Zanotti-Fregonara P, Yu M, Faridar A, Nakawah MO et al. Brain inflammation co-localizes highly with tau in mild cognitive impairment due to early-onset Alzheimer's disease. Brain. 2024.
36. Zanotti-Fregonara P, Pascual B, Rizzo G, Yu M, Pal N, Beers D, et al. Head-to-Head Comparison of (11)C-PBR28 and (18)F-GE180 for Quantification of the Translocator Protein in the Human Brain. J Nucl Med. 2018;59(8):1260–6.
37. Ikawa M, Lohith TG, Shrestha S, Telu S, Zoghbi SS, Castellano S, et al. 11C-ER176, a Radioligand for 18-kDa Translocator Protein, Has Adequate Sensitivity to Robustly Image All Three Affinity Genotypes in Human Brain. J Nucl Med. 2017;58(2):320–5.
38. Fujita M, Kobayashi M, Ikawa M, Gunn RN, Rabiner EA, Owen DR, et al. Comparison of four (11)C-labeled PET ligands to quantify translocator protein 18 kDa (TSPO) in human brain: (R)-PK11195, PBR28, DPA-713, and ER176-based on recent publications that measured specific-to-non-displaceable ratios. EJNMMI Res. 2017;7(1):84.
39. McFadden K, Hamilton RL, Insalaco SJ, Lavine L, Al-Mateen M, Wang G, et al. Neuronal intranuclear inclusion disease without polyglutamine inclusions in a child. J Neuropathol Exp Neurol. 2005;64(6):545–52.
40. Martínez Cerdeño V, Hong T, Amina S, Lechpammer M, Ariza J, Tassone F, et al. Microglial cell activation and senescence are characteristic of the pathology FXTAS. Mov Disord. 2018;33(12):1887–94.
41. Lodygensky GA, West T, Stump M, Holtzman DM, Inder TE, Neil JJ. In vivo MRI analysis of an inflammatory injury in the developing brain. Brain Behav Immun. 2010;24(5):759–67.

Figures

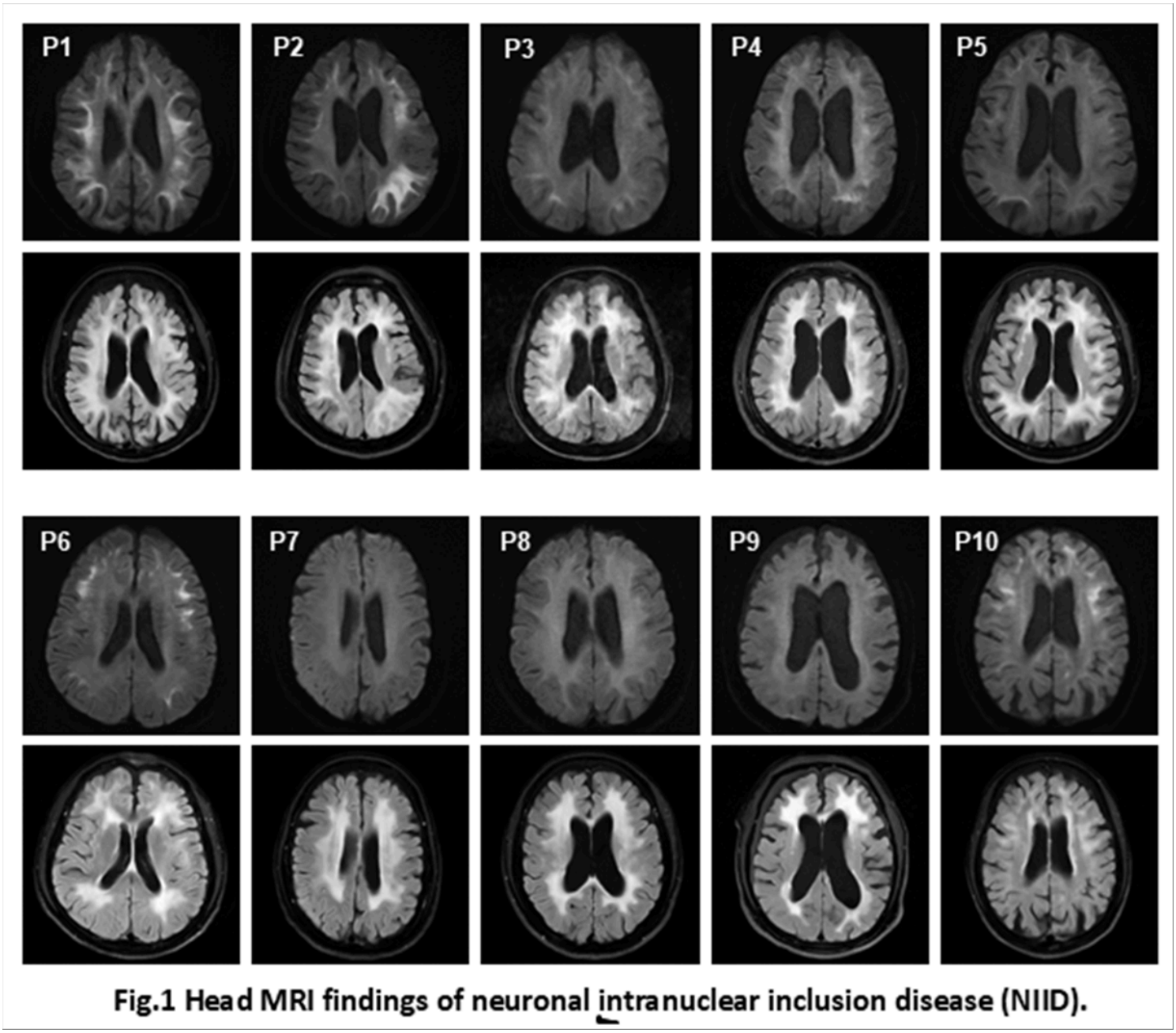

Figure 1

Head MRI findings of in patients with neuronal intranuclear inclusion disease (NIID). Leukoencephalopathy of NIID patients is revealed by DWI (upper panel) and T2-FLAIR sequences

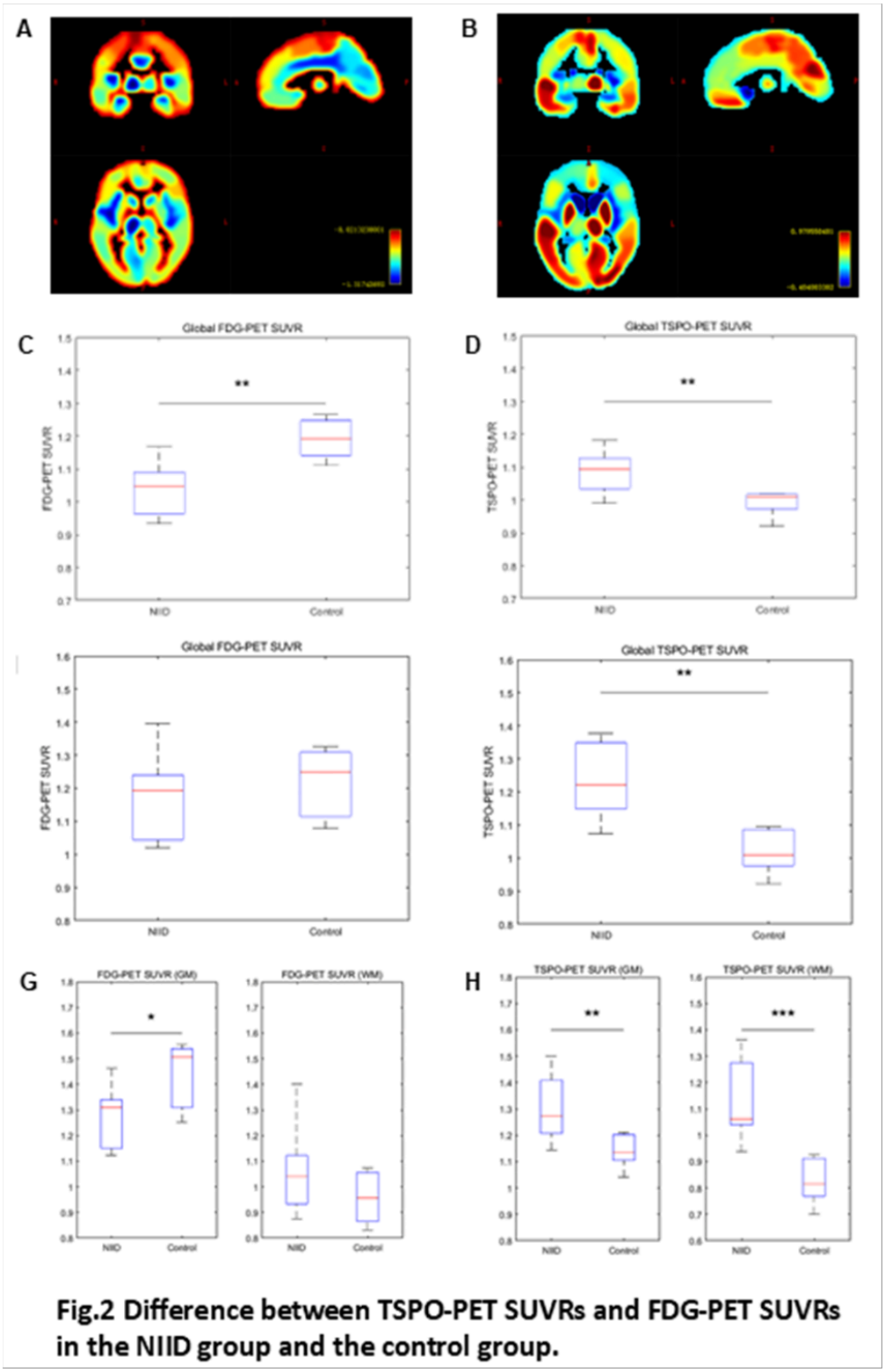

Fig.2 Difference between TSPO-PET SUVRs and FDG-PET SUVRs in the NIID group and the control group.

Figure 2

Difference between TSPO-PET SUVRs and FDG-PET SUVRs in the NIID and the control groups. (A, B) Z-score distribution of FDG-PET SUVR (A) and TSPO-PET SUVR (B) in NIID patients. (C, D) The global FDG-PET SUVRs and TSPO-PET SUVRs in NIID patients and control, defined using the AAL standard brain template (Box-and-whisker plot, min-max; n=10 for NIID and n=5 for control; Mann-Whitney U test). (E, F) The global FDG-PET SUVRs and TSPO-PET SUVRs in NIID patients and control, defined using the individual template (Box-and-whisker plot, min-max; n=10 for NIID and n=5 for control; Mann-Whitney U test). (G) The global FDG-PET SUVRs of gray matter and white matter in NIID patients and control, defined using

the individual template (Box-and-whisker plot, min-max; n=9 for NIID and n=5 for control; Mann-Whitney U test). (H) The global FDG-PET SUVRs of gray matter and white matter in NIID patients and control, defined using the individual template (Box-and-whisker plot, min-max; n=9 for NIID and n=5 for control; Mann-Whitney U test). *p□0.05, **p□0.01

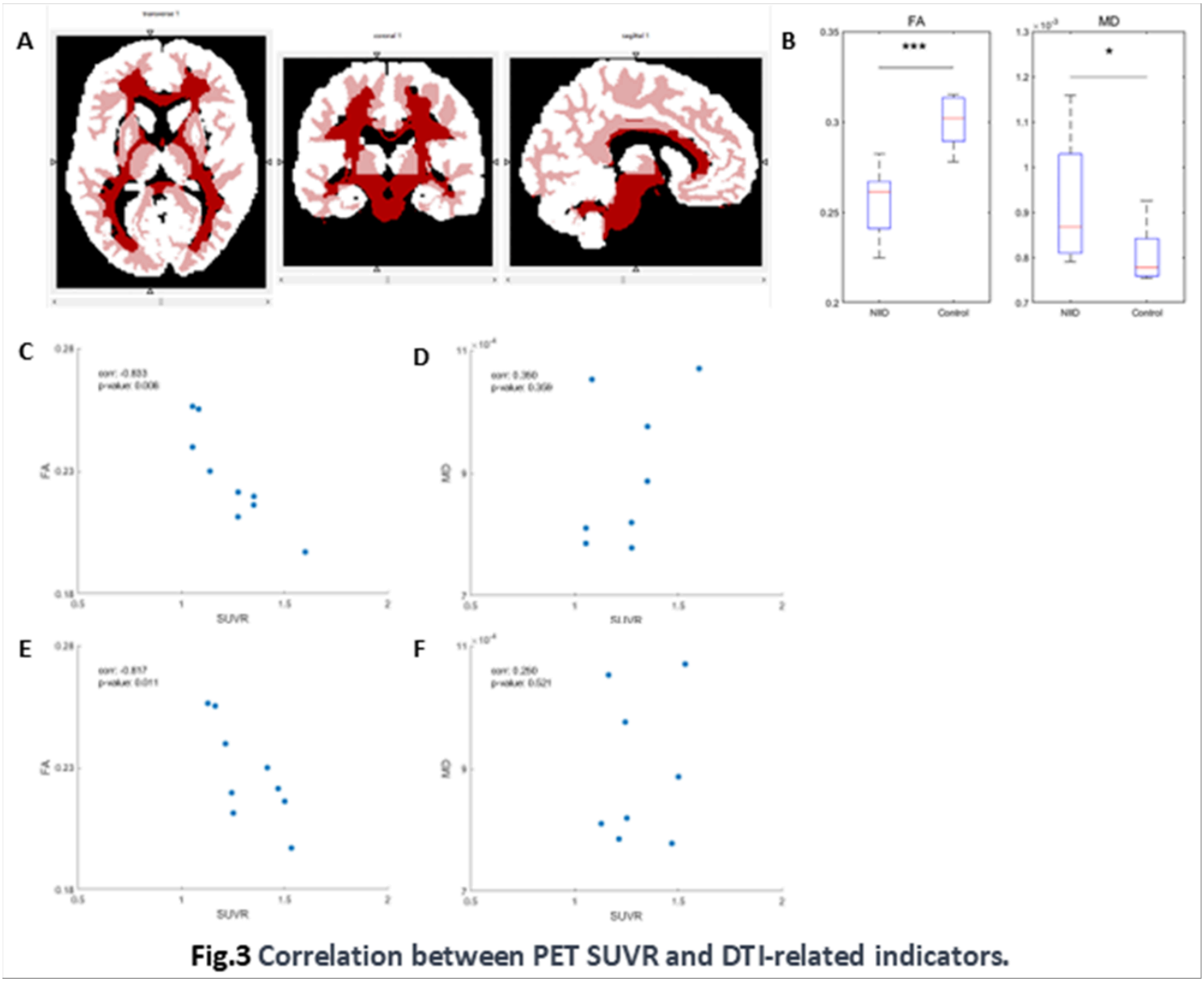

Fig.3 Correlation between PET SUVR and DTI-related indicators.

Figure 3

Correlation between PET SUVR and DTI-related indicators. (A) Region of interest was derived from the overlap between the brain areas defined using the AAL standard brain template and those defined using the individual template, representing superficial white matter (reddish-colored area). (B) The average FA and MD in NIID patients and the control (Box-and-whisker plot, min-max; n=9 for NIID and n=5 for control; Mann-Whitney U test). (C) Correlation of FDG-PET SUVR and DTI FA in the region of interest in NIID patients (n=9 for NIID; Spearman's rank correlation analysis). (D) Correlation of FDG-PET SUVR and MD in the region of interest in NIID patients (n=9 for NIID; Spearman's rank correlation analysis). (E) Correlation of FDG-PET SUVR and DTI FA in the region of interest in NIID patients (n=9 for NIID; Spearman's rank correlation analysis). (F) Correlation of FDG-PET SUVR and MD in the region of interest in NIID patients (n=9 for NIID; Spearman's rank correlation analysis). *p□0.05, **p□0.01, ***p□0.001

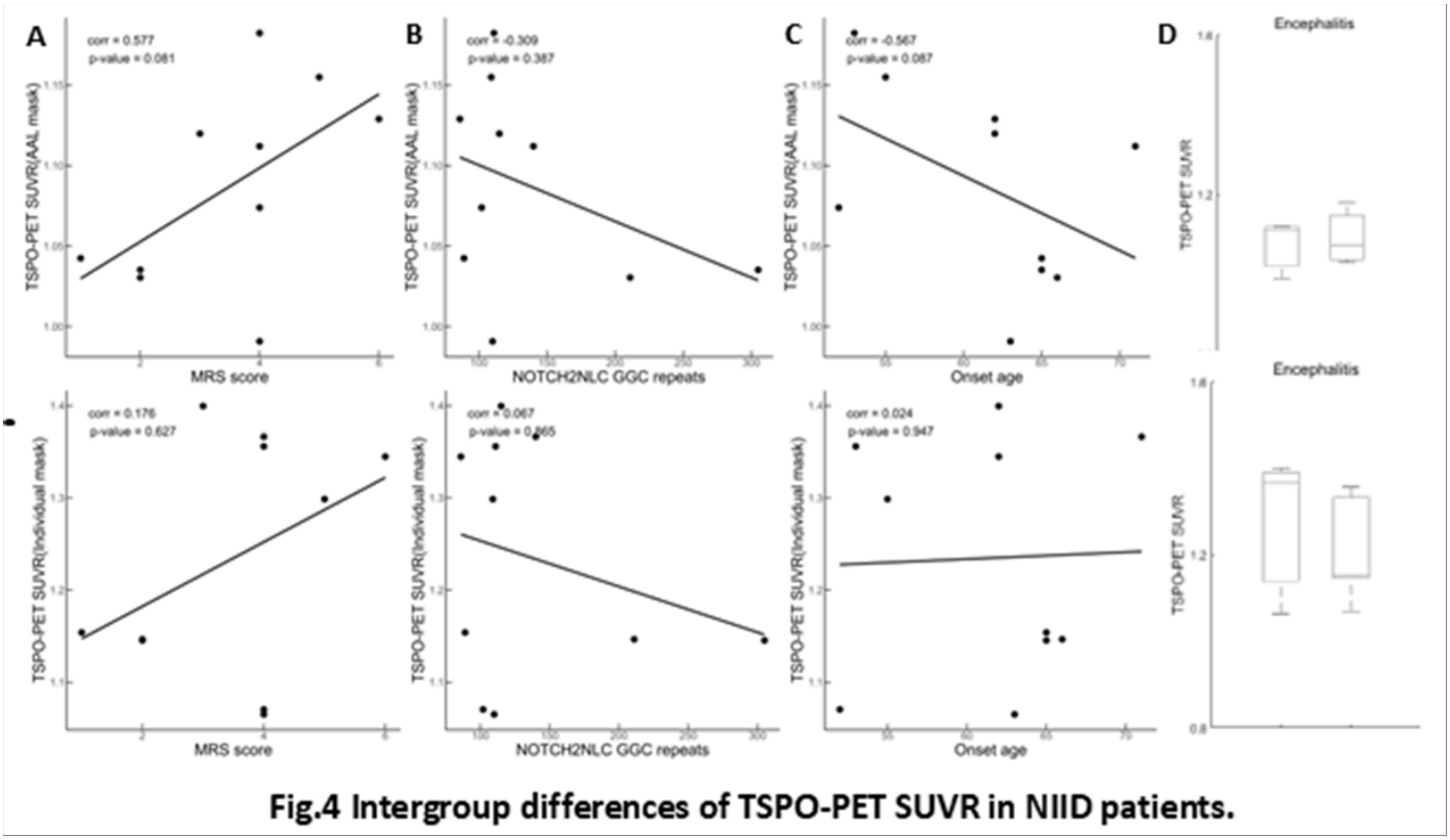

Figure 4

Intergroup differences of TSPO-PET SUVR in NIID patients. (A-C) Correlation between MRS scores (A), GGC repeats (B), age at onset (C), and global TSPO SUVR in NIID patients, defined using the AAL standard brain template (upper panel) and the individual template (lower panel) (n=10 for NIID; Spearman's rank correlation analysis). (D) Global TSPO SUVR in NIID patients with (n=3) or without (n=7) encephalitis-like episodes, defined using the AAL standard brain template (upper panel) and the individual template (lower panel) (Box-and-whisker plot, min-max; Mann-Whitney U test)